



Time-optimal trajectory planning for a race car considering variable tyre-road friction coefficients

Fabian Christ, Alexander Wischnewski, Alexander Heilmeier & Boris Lohmann

To cite this article: Fabian Christ, Alexander Wischnewski, Alexander Heilmeier & Boris Lohmann (2019): Time-optimal trajectory planning for a race car considering variable tyre-road friction coefficients, Vehicle System Dynamics, DOI: [10.1080/00423114.2019.1704804](https://doi.org/10.1080/00423114.2019.1704804)

To link to this article: <https://doi.org/10.1080/00423114.2019.1704804>



Published online: 22 Dec 2019.



Submit your article to this journal [↗](#)



View related articles [↗](#)



View Crossmark data [↗](#)



Time-optimal trajectory planning for a race car considering variable tyre-road friction coefficients

Fabian Christ ^a, Alexander Wischnewski ^a, Alexander Heilmeyer ^b and Boris Lohmann^a

^aChair of Automatic Control, Technical University of Munich, Munich, Germany; ^bChair of Automotive Technology, Technical University of Munich, Munich, Germany

ABSTRACT

This paper shows the planning of time-optimal trajectories, which allows an autonomous race car to drive at the handling limits, taking into account locally changing road friction values. For this purpose, the minimum lap time problem is described as an optimal control problem, converted to a nonlinear programme using direct orthogonal Gauss-Legendre collocation and then solved by the interior-point method IPOPT. Reduced computing times are achieved using a curvilinear abscissa approach for track description, algorithmic differentiation using the software framework CasADi, and a smoothing of the track input data by approximate spline regression. The vehicle's behaviour is approximated as a single track and double track model with quasi-steady state tyre load simplification and nonlinear tyre model. The results are used to evaluate which vehicle physics are important for the calculation of the time-optimal trajectory. The novelty of this work is the consideration of wheel-specific tyre-road friction coefficients along the racetrack using a track friction map. It is shown that variable friction coefficients have a significant impact on the trajectory, and therefore significantly improve lap times on inhomogenous racetracks. The proposed trajectory planning has proven its practical suitability in first tests on an autonomous race car and will be used in the coming racing season in the Roborace competition.

ARTICLE HISTORY

Received 9 June 2019
Revised 27 September 2019
Accepted 18 November 2019

KEYWORDS

Trajectory planning;
numerical optimal control;
nonlinear programming;
variable tyre-road friction
coefficients; autonomous
race car

1. Introduction

The basic goal of any racing sport is to complete a certain number of laps in the minimum possible time. In order to achieve this goal, it is useful to determine the optimal trajectory for a given racetrack, taking into account the physical properties of the racing vehicle. This problem is mostly called the minimum lap time problem (MLTP).

The planning of time-optimal trajectories at the limits of handling is of great practical interest. In racing, it is common to use numerical optimisation methods to determine the lap time for specific race cars. Furthermore, investigations into various design parameters and vehicle setups help to identify performance limits, and thus provide information about possible constructive as well as strategic improvement potentials [1].

The aim of this paper is to study the MLTP allowing an autonomous race car to drive a racetrack at the handling limits. The key contribution is the consideration of variable wheel-specific friction coefficients along the racetrack.

This work was created as part of the Roborace competition, in which the chairs of Automotive Technology and Automatic Control of the Technical University of Munich participate in order to benchmark state-of-the-art software for autonomous cars at the physical limits of a vehicle.

The rest of the paper is structured as follows: Firstly, related work on solving the MLTP with optimal control-based approaches is presented in Chapter 2. Then the track model is introduced in Chapter 3, before vehicle models are discussed in detail in Chapter 4. The description of the trajectory planning ends with the formulation and the numerical solution of the optimal control problem (OCP). Afterwards, simulation results are presented and an outlook is given.

2. Related work

The task of the MLTP is to determine the controls for a selected vehicle and track model that allow the vehicle to be guided around the lap in the shortest possible time [2]. It is a kinodynamic problem. A collision-free path is planned around the racetrack (kinematic boundary condition), while the maximum possible physical velocities and accelerations (dynamic boundary conditions) are simultaneously taken into account [3].

The first lap time simulation was performed by Mercedes in the 1940s [2]. A multitude of different approaches to solving the MLTP has been developed since that time. These mainly differ from one another in their intended use, the simplifications made and their numerical effort. Common methods fall into four categories: quasi-steady state, optimal control-based, driver model-based and evolutionary algorithm-based approaches [3]. In this paper, an optimal control-based approach is used, since these methods offer the possibility of depicting the transient vehicle motion through the use of complex models with average numerical effort at the same time. A multitude of optimal control-based approaches are available that use either the indirect or the direct method of solving the formulated OCP.

The indirect method is based on Pontryagin's Minimum Principle [4], which provides the necessary first-order optimality conditions (differential equations). To solve these, a two-point boundary value problem must be solved in combination with a minimisation problem. Indirect methods thus solve the OCP indirectly by converting the OCP into a boundary value problem, which is then solved numerically [5].

The MLTP was successfully solved with the indirect method for motorcycles, go-karts and vehicles [3,6–10] for which the software PINS [11] has always been used. The suitability of the indirect method for solving the MLTP was determined particularly in [6]. Here, a time-optimal trajectory for a GP2 race car is planned based on a multi-body model with 14 degrees of freedom. It illustrates the structure movements, the movements of the wheel suspension and the wheel rotations. Even with this complex vehicle model, a computing time of 26 minutes is achievable for the whole racetrack in Barcelona.

On the other hand, direct methods first convert the infinite dimensional OCP into a finite dimensional nonlinear programme (NLP) with the help of a transcription method, which is then solved by numerical, iterative optimisation methods. Common transcription

methods are *Direct Single Shooting*, *Direct Multiple Shooting* or *Direct Collocation*. In particular, direct collocation is increasingly used because the resulting NLP can be solved efficiently with the freely available NLP solver IPOPT [12], a primal-dual interior-point method. In addition to interior-point methods (e.g. IPOPT [12]), SQP methods (e.g. SNOPT [13]) are also used.

One of the first optimal control-based publications for solving the MLTP [2] was published in 2000, using a *Direct Multiple Shooting* approach and the NLP solver SNOPT [13]. Here, the MLTP is solved for a Formula One race car modelled as a double track model with a nonlinear tyre model. A whole series of publications on solving the MLTP for a Formula One race car was created based on [14], in which a direct collocation method is used by means of the software ICLOCS2 [15] to determine the influence of different vehicle parameters, such as the position of the vehicle's centre of gravity, on the lap time. The calculation time for the racetrack in Barcelona is about 15 minutes. In [16], this formulation of the MLTP is extended to include an optimal energy management strategy when energy recovery systems are used, while in [17] the interaction between the aerodynamic vehicle performance and the wheel suspension is considered in order to finally perform track-specific parameter optimizations. Finally, in [18] the formulation of the MLTP is enlarged for three-dimensional track surfaces. In [16–18] a global, direct orthogonal collocation is applied using the software GPOPS-II [19] and the NLP solver IPOPT [12].

The literature review shows that indirect and direct methods are both suitable for solving the MLTP. In [3], two state-of-the-art software programmes for solving the MLTP, GPOPS-II [19] (direct method) and PINS [11] (indirect method), are compared and a similar performance is observed. Nowadays, direct methods are more common than indirect methods mainly due to their simple applicability and high robustness, the simple consideration of complex path constraints, the larger convergence range and the freely available NLP Solver IPOPT [12]. Due to these advantages, the direct method is favoured in this work.

Previous approaches assume a constant tyre-road friction coefficient μ along the race-track. This assumption represents a drastic simplification, because the overestimation of adhesion potential of tyres leads directly to safety-critical driving manoeuvres.

3. Track model

3.1. Road and vehicle tracking

The track is modelled using a curvilinear coordinate system that uses the arc length of a reference line as the abscissa. This approach is widely used (e.g. [8,14]).

Referring to Figure 1, the track is described by means of the curvature of the reference line κ and the corresponding track widths to the left (N_l) and right side (N_r). At any point s the curvature κ is given by the inverse of the local radius of curvature R . The tangent vector on the reference line t is described by the track orientation angle θ . The location and orientation of the vehicle can be described by the curvilinear abscissa along the reference line s , the lateral displacement from the reference line n and the relative angle between the tangent vector and the vehicle orientation ξ . The direction of the velocity vector v is described by the side slip angle β .

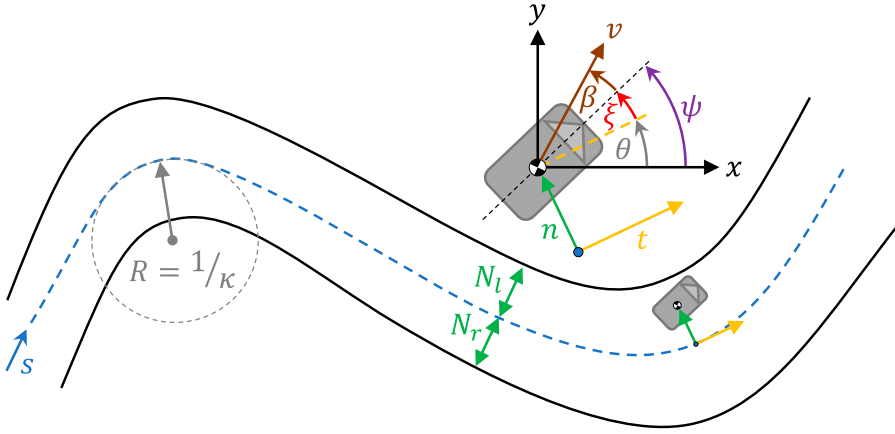


Figure 1. Road and vehicle position are described by curvilinear abscissa s , curvature of reference line κ , track widths N_l and N_r , lateral displacement from reference line n and relative angle ξ .

The equations describing the time evolution of the introduced coordinates s , n and ξ are [20]:

$$\dot{s} = \frac{v \cos(\xi + \beta)}{1 - n\kappa}, \quad (1a)$$

$$\dot{n} = v \sin(\xi + \beta), \quad (1b)$$

$$\dot{\xi} = \omega_z - \kappa \frac{v \cos(\xi + \beta)}{1 - n\kappa}, \quad (1c)$$

where ω_z is the yaw rate.

3.2. Change of independent variable

In race line optimisation, it is common to use the path coordinate s as an independent variable [2,3,8,14,16,17,20,21]. The time to be optimised is therefore a dependent variable. This choice enables a compact description of the vehicle progress along the racetrack, a simple consideration of the track boundaries and the start and end conditions as well as a simple introduction of variable parameters along the racetrack [14]. Finally, s is no longer required as a state variable, reducing the problem size and saving computing time.

The choice of the independent variable, however, requires an adaptation of the OCP formulation. Therefore, the relationship between the time increment dt and the corresponding increment of the travelled distance ds measured along the reference line is given by [20]:

$$SF = \frac{dt}{ds} = \frac{1 - n\kappa}{v \cos(\xi + \beta)}. \quad (2)$$

Consequently the Lagrange cost function of the OCP to be minimized $\int_{t_0}^{t_f} dt$ can be transformed to $\int_{s_0}^{s_f} SF ds$. Besides, SF enables to transform the system equations formulated in the time domain.

3.3. Extracting track data

The recording of the racetrack (center line and road boundaries) can be performed, for example, by using differential gps [22] or by evaluating 2D-LiDAR data. We use the latter whereby the procedure for obtaining the x_i , y_i coordinates of the centre line with corresponding track widths is described in [23]. Based on this information the curvature κ can be determined numerically by the change of the track orientation angle θ in relation to the change of the arc length s . Unfortunately, the curvature of the centre line usually shows high-frequency oscillations, which is counterproductive in terms of the robustness and the numerical effort of the optimisation. Therefore, the reference line is preprocessed before it is handed over to the optimisation problem.

Common approaches try to solve this problem by minimising the first and second derivatives of the line curvature by means of a quadratic optimisation problem [20] or by solving an additional OCP in order to find the curvature of the centre line [3,14].

In contrast to these approaches we perform an approximate spline regression and generate a smooth reference line, which varies slightly from the centre line, and thus offers more scope for action in the smoothing procedure. The methodology is presented in [23].

4. Vehicle models

In the following section, a single track model and a double track model are introduced for comparison purposes. The derivation of the model equations is based on [24].

4.1. Double track model

4.1.1. Dynamic model

The double track model used here is set up with longitudinal, lateral and yaw freedoms. It mainly combines a nonlinear tyre model, an approximate description of the engine characteristic [20] and a quasi-steady state wheel load transfer [14]. The free-body diagram of the double track model with important modelling quantities is depicted in Figure 2.

The OCP solution strategy used in this work requires the model dynamics to be described by a set of first-order ordinary differential equations. They are given by:

$$\dot{v} = \frac{1}{m} \left((F_{x,rl} + F_{x,rr}) \cos(\beta) + (F_{x,fl} + F_{x,fr}) \cos(\delta - \beta) + (F_{y,rl} + F_{y,rr}) \sin(\beta) - (F_{y,fl} + F_{y,fr}) \sin(\delta - \beta) - \frac{1}{2} c_d \rho A v^2 \cos(\beta) \right), \quad (3a)$$

$$\dot{\beta} = -\omega_z + \frac{1}{mv} \left(-(F_{x,rl} + F_{x,rr}) \sin(\beta) + (F_{x,fl} + F_{x,fr}) \sin(\delta - \beta) + (F_{y,rl} + F_{y,rr}) \cos(\beta) + (F_{y,fl} + F_{y,fr}) \cos(\delta - \beta) + \frac{1}{2} c_d \rho A v^2 \sin(\beta) \right), \quad (3b)$$

$$\dot{\omega}_z = \frac{1}{J_{zz}} \left((F_{x,rr} - F_{x,rl}) \frac{t w_r}{2} - (F_{y,rl} + F_{y,rr}) l_r \right)$$

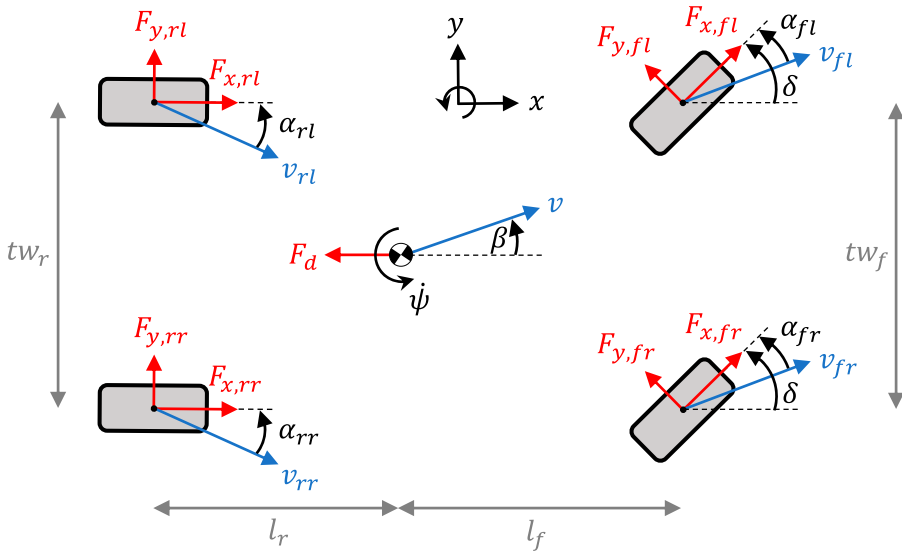


Figure 2. Double track model.

$$\begin{aligned}
 &+ \left((F_{x,fr} - F_{x,fl}) \cos(\delta) + (F_{y,fl} - F_{y,fr}) \sin(\delta) \right) \frac{tw_f}{2} \\
 &+ \left((F_{y,fl} + F_{y,fr}) \cos(\delta) + (F_{x,fl} + F_{x,fr}) \sin(\delta) \right) l_f \Big). \quad (3c)
 \end{aligned}$$

(3a) and (3b) describe the longitudinal and lateral momentum with respect to the centre of gravity, while Equation (3c) refers to the yaw motion. The state variables are the velocity at the centre of gravity v , the side slip angle β and the yaw rate ω_z . Here, m denotes the vehicle mass, J_{zz} the mass moment of inertia with respect to the vertical axis, l the wheelbase, l_f and l_r the distances between centre of gravity and the front and rear axle, while tw_f and tw_r describe the track widths at the front and rear axle respectively. Tyre forces are divided into longitudinal $F_{x,ij}$ and lateral forces $F_{y,ij}$ where the first index i chooses between the front and rear axle, while index j distinguishes between left and right side of the vehicle. The aerodynamic drag force is assumed to be quadratic in the vehicle speed and is applied at the centre of pressure, which is located at the vehicle's centre of gravity for the sake of simplicity. ρ denotes the air density, A the frontal area of the vehicle and c_d is the aerodynamic drag force coefficient. Aerodynamic side forces, yawing moments and pitching effects have been neglected.

The steering angle δ and the longitudinal force, split up into driving force $F_{\text{drive}} \geq 0$ and a braking force $F_{\text{brake}} \leq 0$, are selected as control variables. This choice makes it possible to avoid using non-smooth functions to differentiate between positive and negative longitudinal forces [20].

The braking forces are distributed between the front and the rear axles via the static brake force distribution k_{brake} , while k_{drive} distributes the driving force. The longitudinal tyre forces $F_{x,ij}$ give

$$F_{x,ij} = \frac{1}{2} k_{\text{drive}} F_{\text{drive}} + \frac{1}{2} k_{\text{brake}} F_{\text{brake}} - \frac{1}{2} f_r m g \frac{l_r}{l}, \quad (4a)$$

$$F_{x,rj} = \frac{1}{2} (1 - k_{\text{drive}}) F_{\text{drive}} + \frac{1}{2} (1 - k_{\text{brake}}) F_{\text{brake}} - \frac{1}{2} f_r m g \frac{l_f}{l}, \quad (4b)$$

where the last term in the equations above depicts the rolling resistance, calculated with a static rolling resistance coefficient f_r and the gravitational acceleration g .

4.1.2. Tyre forces

The lateral tyre forces $F_{y,ij}$ are determined using a simplified version of Pacejka's magic formula $F_y = \mu F_z \sin(C \arctan(B\alpha - E(B\alpha - \arctan(B\alpha))))$ using the constant coefficients B , C , E , the slip angle α , the friction coefficient μ and the wheel load F_z . The comparison in Figure 3(a) with a complex tyre model (dotted line) shows that the simple model overestimates the transferable lateral tyre forces F_y of the tyre, especially at high normal forces F_z . To avoid too high lateral tyre forces F_y , the tyre model is extended as follows:

$$F_{y,ij} = \mu_{ij} F_{z,ij} \left(1 + \epsilon_i \frac{F_{z,ij}}{F_{z,0}} \right) \sin \left(C_i \arctan \left(B_i \alpha_{ij} - E_i (B_i \alpha_{ij} - \arctan(B_i \alpha_{ij})) \right) \right). \quad (5)$$

Here, the coefficient $\epsilon \leq 0$ introduces a degressive tyre behaviour against the wheel load. The improved mapping of the front tyre behaviour is shown in Figure 3(b). μ_{ij} describes the variable wheel-specific friction coefficient along the racetrack.

The tyre sideslip angles α_{ij} are calculated by kinematic relations as follows [25]:

$$\alpha_{fl/fr} = \delta - \arctan \left(\frac{l_f \omega_z + v \sin(\beta)}{v \cos(\beta) \mp \frac{1}{2} t w_f \omega_z} \right), \quad (6a)$$

$$\alpha_{rl/rr} = \arctan \left(\frac{l_r \omega_z - v \sin(\beta)}{v \cos(\beta) \mp \frac{1}{2} t w_r \omega_z} \right). \quad (6b)$$

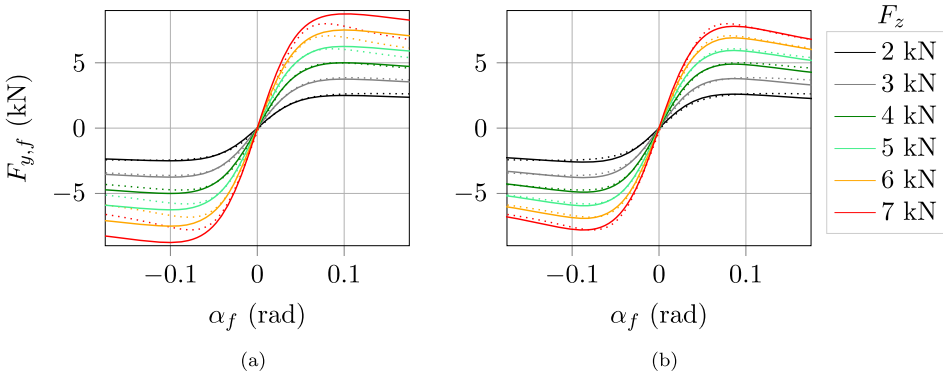


Figure 3. Nonlinear tyre models for calculating the lateral forces $F_{y,ij}$. (a) Pacejka magic formula without consideration of the tyre degression against the normal force F_z . (b) Pacejka magic formula with consideration of the tyre degression against the normal force F_z .

The vertical tyre load $F_{z,ij}$ consists of a static as well as dynamic terms, and is approximated by

$$F_{z,fl/fr} = \frac{1}{2}mg \frac{l_r}{l_f + l_r} - \frac{1}{2} \frac{h_{\text{cog}}}{l_f + l_r} ma_x \mp k_{\text{roll}} \Gamma_y + \frac{1}{4} c_{l,f} \rho A v^2, \quad (7a)$$

$$F_{z,rl/r} = \frac{1}{2}mg \frac{l_f}{l_f + l_r} + \frac{1}{2} \frac{h_{\text{cog}}}{l_f + l_r} ma_x \mp (1 - k_{\text{roll}}) \Gamma_y + \frac{1}{4} c_{l,r} \rho A v^2, \quad (7b)$$

where a_x and a_y denote the longitudinal and lateral acceleration at the centre of gravity, h_{cog} the height of the centre of gravity and Γ_y the lateral wheel load transfer. The dynamic portion is calculated from the aerodynamic downforce and the dynamic wheel load shift. The aerodynamic down force is assumed to be quadratic in the vehicle speed and is applied to the front and rear axle separately in the car's plane of symmetry. The constants $c_{l,i}$ denote the lift coefficients for the front and rear axles respectively [26]. The vehicle is regarded as a rigid body without elastic wheel suspension. This leads to an instantaneous change in the wheel loads during vehicle acceleration. Using the common quasi-steady state wheel load transfer simplification, k_{roll} denotes a suspension-related roll balance relationship, in which the lateral load difference across the front axle is a certain fraction of the total lateral load difference. Γ_y quantifies the dynamic wheel load change, which relieves the left (right) half of the vehicle by Γ_y and additionally loads the right (left) half of the vehicle by Γ_y and is calculated using the current lateral acceleration a_y and the geometric dimensions of the vehicle:

$$\Gamma_y = \frac{h_{\text{cog}}}{\frac{1}{2}(tw_f + tw_r)} (F_{y,rl} + F_{y,rr} + (F_{x,fl} + F_{x,fr}) \sin(\delta) + (F_{y,fl} + F_{y,fr}) \cos(\delta)). \quad (8)$$

This shows that the normal tyre forces $F_{z,ij}$ caused by the chosen calculation rule for Γ_y depend on the lateral tyre forces $F_{y,ij}$, which in turn depend on the normal tyre forces $F_{z,ij}$. This algebraic loop can be bypassed by defining the lateral wheel load transfer Γ_y as a new control variable. The calculation rule for Γ_y can then be considered as an equality constraint.

For simple implementation and to ensure short computing times, the longitudinal acceleration a_x is approximated for the steering angle $\delta = 0$ [20], whereby a_x can be specified as a function of the state and control variables:

$$ma_x \approx F_{\text{drive}} + F_{\text{brake}} - \frac{1}{2} c_d A v^2 - f_r mg. \quad (9)$$

The Pacejka tyre model presented allows the lateral tyre force F_y to be calculated as a function of the normal force F_z and the tyre slip angle α for a pure lateral force load. For a good illustration of the transferable tyre forces, the pure longitudinal force load as well as the combined load case must also be considered. For this purpose, the descriptive modelling with Kamm's circle is often used [3,20]. The radius of Kamm's circle corresponds to the maximum transmittable horizontal force $\mu \cdot F_z$ that the tyre can transmit without sliding. This maximum value must not be exceeded either by pure longitudinal or lateral force loading or by combined loading, where in the combined load case the resulting horizontal force is calculated by $\sqrt{F_x^2 + F_y^2}$ [27]. This requirement is formulated for each of the four

tyres along the trajectory by the following inequality constraint:

$$\left(\frac{F_{x,ij}}{\mu_{ij} \cdot F_{z,ij}} \right)^2 + \left(\frac{F_{y,ij}}{\mu_{ij} \cdot F_{z,ij}} \right)^2 \leq 1. \quad (10)$$

μ_{ij} represents the friction coefficient for each of the four wheels along the racetrack, whose calculation is presented in Section 4.3.

4.1.3. Static actuator constraints

For a realistic representation of the vehicles behaviour it is necessary to consider the actuator properties. In the present vehicle, two electric motors are used on the rear axle, allowing the drive torques to be applied evenly between the left and right sides. Since the problem at hand is an electric motor without gear shifting, the engine map can be approximated by introducing two inequality constraints for the driving force F_{drive} and the power $P = v \cdot F_{\text{drive}}$:

$$v \cdot F_{\text{drive}} \leq P_{\text{max}}, \quad (11a)$$

$$F_{\text{drive}} \leq F_{\text{drive,max}}. \quad (11b)$$

The splitting of the longitudinal force into a driving force F_{drive} and a braking force F_{brake} requires the introduction of the equality constraint

$$F_{\text{drive}} \cdot F_{\text{brake}} = 0 \text{ N}^2 \quad (12)$$

to prevent brake and drive from being actuated simultaneously. In practice, this requirement is eased slightly by an inequality constraint [20].

The steering angle δ is also limited. The maximum available steering angle range can be specified by the inequality constraint

$$-\delta_{\text{max}} \leq \delta \leq \delta_{\text{max}}, \quad (13)$$

where δ_{max} corresponds to half of the maximum steering angle range available.

4.1.4. Dynamic actuator constraints

In addition to compliance with the maximum permissible values for the control variables, the actuator dynamics of the vehicle must also be taken into account. Detailed modelling of the steering and powertrain dynamics is dispensed in order to keep model complexity low. Instead, only the rates of change of the control variables are limited. The dynamic limitations can be introduced by formulating the following inequality constraints [20]:

$$\frac{F_{\text{drive},k+1} - F_{\text{drive},k}}{SF_k \cdot \Delta s} \leq \frac{F_{\text{drive,max}}}{T_{\text{drive}}}, \quad (14a)$$

$$\frac{F_{\text{brake},k+1} - F_{\text{brake},k}}{SF_k \cdot \Delta s} \geq \frac{F_{\text{brake,max}}}{T_{\text{brake}}}, \quad (14b)$$

$$\frac{-\delta_{\text{max}}}{T_{\delta}} \leq \frac{\delta_{k+1} - \delta_k}{SF_k \cdot \Delta s} \leq \frac{\delta_{\text{max}}}{T_{\delta}}. \quad (14c)$$

4.2. Single track model

The single track model is based on equations similar to those of the double track model. They can be determined by merging the wheels of an axle. The main difference lies in the neglect of the lateral wheel load transfer Γ_y and differences due to kinematic relations. For the sake of simplicity, and due to the similarity to the double track model, the single track model is not presented.

4.3. Variable tyre-road friction coefficients

Approaches found in literature assume a constant tyre-road friction coefficient μ along the racetrack. This assumption represents a drastic simplification in practical application because the overestimation of adhesion potential of tyres leads directly to safety-critical driving manoeuvres. For this reason, a new method is presented, which allows a discretised friction map given in cartesian coordinates (x_i - y_i - μ_i) to be considered in the OCP.

The influences on the friction coefficient are manifold and various methods exist for acquiring variable tyre-road friction coefficients [28]. The estimation of a solid database for the friction map is the subject of current research. A corresponding publication will soon be published on this topic [29]. For the purposes of the following investigations, we assume that the tyre-road friction coefficients are known precisely for the racetrack.

Figure 4(a) shows an exemplary friction map for a track section superimposed by the discretization scheme used to describe the position of the vehicle's centre of gravity in the OCP formulation. The position of the centre of gravity can vary continuously along the green-coloured normals.

For these investigations, path limitations, such as the limitation of the traction potential, are formulated at the interval boundaries along the discretised path coordinate s . Therefore, the discretization length Δs is decisive for the approximation of possible abrupt changes of the static friction value along the racetrack.

The basic idea is to express the static friction values μ_{ij} at each path coordinate s_k depending on the NLP decision variables that determine the position of the tyres. The

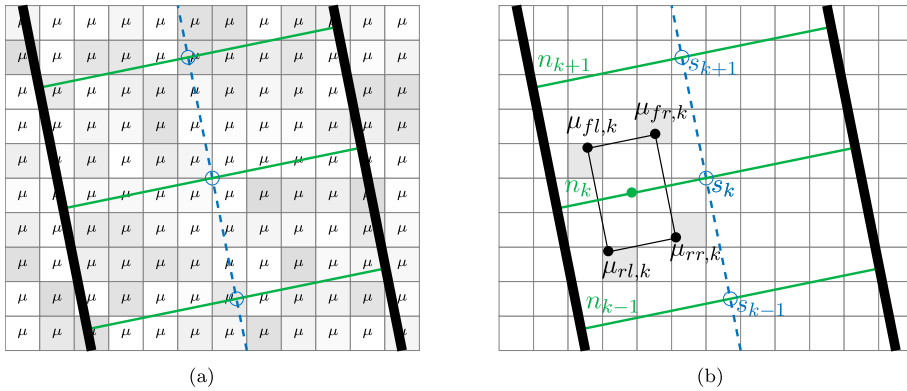


Figure 4. Extracting wheel-specific friction coefficients $\mu_{ij,k}$ from the friction map. (a) Possible positions of the vehicle's centre of gravity in the friction map. (b) Extract friction coefficients for each wheel on a discretised vehicle position.

vehicle position and orientation are given at each path coordinate s_k by the orthogonal distance n and the relative angle ξ . The vehicle dimensions also determine the tyre positions of the double track model. Since the relative angle ξ assumes only small values, the position of the tyres in the friction map can be determined by the state variable n for the sake of simplicity.

To obtain a simplified dependency between the friction coefficients μ_{ij} and the lateral distance n , friction coefficients μ_{ij} are determined for a fine grid on n (e.g. $\Delta n = 0.1$ m) from the friction map. Figure 4(b) shows one of these calculations for the path coordinate s_k .

Then the dependency between the extracted friction coefficients μ_{ij} and the decision variable n for each path coordinate s_k must be described by a continuous function. The selection of the function class has a strong influence on the quality of the mapping of the friction map. A very simple representation can be achieved using the simple linear regression. For highly dynamic friction maps, a linear regression with gaussian basis functions is useful:

$$\mu_{ij,k}(s_k) = \sum_{q=1}^{n_{\text{gauss}}} w_{ij,k,q} \cdot e^{-(n_k - n_q)^2 / 2\sigma^2}. \quad (15)$$

The coefficients $w_{ij,k,q}$ for the superposition of n_{gauss} gaussian basis functions must be calculated for each tyre and for each path coordinate s_k . The shape of the gaussian basis functions is determined by their width σ and their lateral position n_q .

Figure 5 shows these two approximation methods to describe the dependency between the extracted friction coefficients μ_{ij} and the decision variable n for the path coordinate s_k . It is shown that the gaussian basis functions are much better suited for the approximation of variable friction coefficients across the reference line.

This method allows variable friction coefficients to be considered along the racetrack. The simplifications used are the neglect of the relative angle ξ , the approximation of the friction coefficients along the normals and the formulation on the grid s_k . In principle, the formulation of path restrictions is also conceivable at the collocation points between the interval boundaries, although the numerical accuracy is lower.

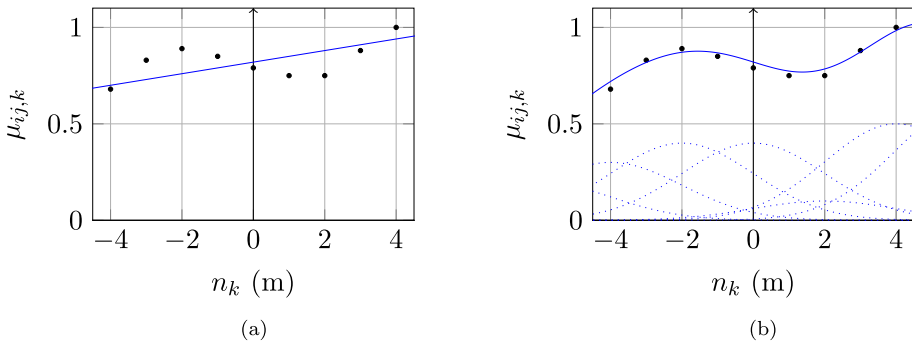


Figure 5. Approximation of a tyre-road friction coefficient μ_{ij} at the path coordinate s_k with continuous functions. (a) Approximation with linear equation. (b) Approximation with gaussian basis functions.

The methodology presented above is only used to limit the transmittable horizontal tyre forces according to Equation (10). For the calculation of the lateral tyre forces $F_{y,ij}$ according to Equation (5), μ is instead only varied along the reference line and not described in dependence of the lateral distance n . This simplification prevents the collocation equations for implementing the system dynamics from becoming more complex and causing high computing times. This is sufficient, since the exact course of the control variables is not required for the present application.

5. Numerical optimal control

5.1. Optimal control problem formulation

The formulation of the OCP for the MLTP is presented in the following general form:

$$\min_{x,u} \int_{s_0}^{s_f} L(x(s), u(s)) ds \quad (16a)$$

$$\text{s.t.} \quad \frac{dx}{ds} - f(x(s), u(s)) = 0, \quad (16b)$$

$$g(x(s), u(s)) = 0, \quad (16c)$$

$$h(x(s), u(s)) \leq 0, \quad (16d)$$

$$r(x(s_0), x(s_f)) \leq 0, \quad (16e)$$

where s , the independent variable of the optimal control problem, is the distance travelled along the reference line and extends from the start (s_0) to the finish line (s_f) of the racetrack. $x(s) \in \mathbb{R}^{n_x}$ and $u(s) \in \mathbb{R}^{n_u}$ denote the vehicle state and control vectors, respectively. The system dynamics, described by the vector function $f(\cdot) \in \mathbb{R}^{n_x}$, are met by (16b). The system equations have been presented in the time domain so far. Therefore, a transformation of the equations by multiplication with SF is necessary. Furthermore, the optimal control problem is constrained by equality constraints (16c), described by the vector function $g(\cdot) \in \mathbb{R}^{n_g}$ and inequality constraints (16d), described by the vector function $h(\cdot) \in \mathbb{R}^{n_h}$. The boundary constraints (16e) are met by $r(\cdot) \in \mathbb{R}^{n_r}$. For the solution of the OCP, the course of the control variables is sought, which minimises the Lagrange cost function $L(\cdot) = SF$ (16a) and complies with the restrictions mentioned above.

When using the double track model, $f(\cdot)$ contains (1b), (1c), (3), (4), (5), (6), (7) and (9) with the corresponding states $n, \xi, v, \beta, \omega_z$ and controls $\delta, F_{\text{drive}}, F_{\text{brake}}, \Gamma_y$. Equations (8) and (12) are formulated as equality constraints, whereas (10), (11), (13) and (14) are described as inequality constraints.

The following explanations are valid for both models. An essential path constraint is the consideration of the track boundaries. Compliance with this restriction is mandatory, since an injury may lead to an accident. Since the relative angle ξ usually assumes very small values, the compliance with the track boundaries can be ensured by the following inequality constraint:

$$N_l - \frac{b}{2} - b_{\text{safe}} \geq n \geq -N_r + \frac{b}{2} + b_{\text{safe}}, \quad (17)$$

where the vehicle width b is increased by a safety margin b_{safe} for practical use.

Beside the limitation of the state variable n , a limitation of the velocity v is made. This excludes negative velocities and prevents a specified maximum velocity v_{\max} from being exceeded by $0 \text{ m/s} \leq v \leq v_{\max}$. This upper bound v_{\max} can be set if the application requires a static speed limit (e.g. for test drives), otherwise it is not required as the speed is already limited by the engine power. To obtain a closed race line, the optimisation is performed from the starting point $x(s_0)$ to the end point $x(s_N)$, which corresponds to the starting point: $x(s_N) = x(s_0)$.

5.2. Transcription

To solve the formulated dynamic optimisation problem, a direct numerical solution method is used. Direct methods transform the original, infinitely dimensional OCP into a finitely dimensional NLP, which can then be solved with common numerical methods of nonlinear optimisation.

In this work a simultaneous method is used to fully discretise both the control and state variables using direct local collocation. The trajectories of the control and state variables are discretised on a fine grid s_k with $k = 0, \dots, N$. N corresponds to the number of the discretization intervals and results from the horizon $s_f - s_0$ and the uniform step size Δs . x_k and u_k denote the discrete states and control variables at the interval boundaries s_k . The control variables $u(s)$ are selected as piecewise constant, whereby their courses are defined in the interval $[s_k, s_{k+1}]$ with the parameter u_k (decision variables of the NLP). The trajectories of the state variables $x(s)$ are approximated by a polynomial $P_k(s, \theta_k)$ for each interval $[s_k, s_{k+1}]$ by superposition of Lagrange basis polynomials $p_{k,i}$ multiplied by the coefficients $\theta_{k,i}$ (decision variables of the NLP):

$$P_k(s, \theta_k) = \sum_{i=0}^d \theta_{k,i} \cdot p_{k,i}(s). \quad (18)$$

The Lagrange polynomials $p_{k,i}(t)$ of order d are calculated with the collocation points $s_{k,j}$ with $j = 0, \dots, d$ as follows [30]:

$$p_{k,i}(s) = \prod_{j=0, j \neq i}^d \frac{s - s_{k,j}}{s_{k,i} - s_{k,j}} \in \mathbb{R}. \quad (19)$$

For this problem the Gauss-Legendre collocation is used, in which the collocation points correspond to the zeros of the orthogonal Legendre polynomials. This allows exact integration if the solution x is a polynomial of order $< 2d$ [30]. According to [30] orders $d > 4$ can be counterproductive in practical applications, therefore $d = 3$ is chosen for the present problem. The direct orthogonal collocation scheme transforms the OCP (16) to the following large scale, but sparse NLP:

$$\min_{\theta, u} \sum_{k=0}^{N-1} l_k(\theta_k, u_k) \quad (20a)$$

$$\text{s.t. } \theta_{0,0} - x_{\text{start}} = 0, \quad (20b)$$

$$\dot{P}_k(t_{k,j}, \theta_k) - \Delta s f(\theta_{k,j}, u_k) = 0, \quad k = 0, \dots, N-1, \quad j = 1, \dots, d, \quad (20c)$$

$$P_k(t_{k+1}, \theta_k) - \theta_{k+1,0} = 0, \quad k = 0, \dots, N-1, \quad (20d)$$

$$h(\theta_{k,0}, u_k) \leq 0, \quad k = 0, \dots, N-1, \quad (20e)$$

$$r(\theta_{0,0}, \theta_{N,0}) \leq 0. \quad (20f)$$

In the following, the specific parts of (20) are explained in detail with references to the original parts of the OCP formulation (16):

(20a): To approximate the Lagrange cost function of the OCP (16a), a numerical integration scheme is used, which uses the collocation points $s_{k,j}$. The selected calculation rule is as follows:

$$\int_{s_0}^{s_f} L(x(s), u(s)) ds \approx \sum_{k=0}^{N-1} \Delta s \sum_{r=0}^d B_r L(\theta_{k,r}, u_k), \quad (21)$$

where $B_r = \int_0^1 p_r(\tau) d\tau$ is the integral of the Lagrange basis polynomials [31].

(20b): An equality constraint ensures a continuous transition at the initial starting point x_{start} .

(20c): For the consideration of system dynamics (16b) in the form of equality constraints in the NLP, the coefficients of the polynomial θ_k are determined such that the derivatives of the polynomial correspond to the system dynamics $\dot{x}(s) = f(x(s), u(s))$ at the collocation points $s_{k,j}$.

(20d): In order to ensure a continuous course of the state variables, continuity conditions are introduced, which ensure a continuous transition at the interval boundaries.

(20e): Path constraints $h(x(s), u(s)) \leq 0$ (16d) are usually formulated only for the grid s_k to limit the number of inequality constraints in the NLP, leading to $h(x_k, u_k) \leq 0$ [30].

(20f): Boundary constraints $r(x(s_0), x(s_f)) \leq 0$ (16e) are formulated with respect to the polynomial coefficients $\theta_{0,0}$ and $\theta_{N,0}$, which denote $x(s_0)$ and $x(s_N)$ respectively.

The resulting number of decision variables is very large, but the differential equations are already available as equation constraints and do not require separate integration. The decision variables w of the NLP are:

$$w = (\theta_{0,0}, \dots, \theta_{0,d}, u_0, \dots, \theta_{N-1,0}, \dots, \theta_{N-1,d}, u_{N-1}). \quad (22)$$

The presented NLP (20) can be efficiently solved by SQP or interior point methods. Here, interior point methods are usually faster because the solution of a thin, linear system of equations required in each iteration is usually more favourable than the solution of a quadratic optimisation problem when the derivative evaluations are cheap as it is with direct collocation [30]. Interior point algorithms such as IPOPT [12] need first and second-order derivative information for the functions defining the cost and constraints. The algorithmic differentiation (AD) offers a favourable supply of the necessary derivatives for the large scale NLP resulting from the direct collocation. A widespread combination is therefore the use of direct collocation with the NLP solver IPOPT [12]. This combination is used in this paper with the help of the software framework CasADi [32].

5.3. Scaling

The formulation of an OCP often contains states, control variables or parameters, which can assume very different values. These differences result in entries with different orders in

the Jacobian and Hessian matrix and worsen the convergence behaviour. Scaling is therefore of great importance and has a direct influence on the convergence rate, the termination conditions and the numerical conditioning of the NLP [33]. Therefore, a normalisation of the state and control variables is performed. The scaling is constantly selected for all discretization points and determined on the basis of the expected maximum values of the state and control variables [31]. The scaled state and control variables assume values in the range $[-1, 1]$. The differential equations are scaled by using the same factors.

5.4. Regularization

When OCPs are solved, it is possible that singular arcs exist if control variables enter the system dynamics and the performance index linearly [17]. In order to avoid possible oscillations in the solutions and convergence problems with singular problems, it is often useful to introduce regularisation terms in the cost function.

Regularization terms can be also used to smooth the progression of the control variables. Noisy courses of the control variables result mainly from the quasi-stationary simplifications in the calculation of tyre forces and wheel load transfer. Thus the smoothing can be physically motivated, as the tyre, whose dynamic running-in effects have been neglected so far, cannot react to rapidly changing control values. The tyre model used therefore needs smooth control inputs. Furthermore, the smoothing of the controls is advantageous if the calculated control variables are used as feedforward control input for following the planned race line.

Instead of the usual procedure of regularisation with the control variables u [18], the derivatives of the control variables du/ds are used. The grid for the approximation of the differential equations is uniform. Therefore, it is sufficient to add the euclidean norm of the derivative of the control variables with a regularisation parameter r . The derivation is calculated by multiplying the differentiation matrix

$$D = \begin{bmatrix} 1 & -1 & 0 & 0 & \dots & 0 \\ 0 & 1 & -1 & 0 & \dots & 0 \\ \vdots & \ddots & \ddots & \ddots & \ddots & \vdots \\ 0 & \dots & 0 & 1 & -1 & 0 \\ 0 & 0 & \dots & 0 & 1 & -1 \\ -1 & 0 & 0 & \dots & 0 & 1 \end{bmatrix} \quad (23)$$

with the column vector containing the corresponding control variables of the NLP.

Finally, the cost function can be extended as follows:

$$\begin{aligned} \min \int_{s_0}^{s_f} SF ds + r_\delta [\delta_0, \dots, \delta_{N-1}] D^T D [\delta_0, \dots, \delta_{N-1}]^T \\ + r_F [F_0^*, \dots, F_{N-1}^*] D^T D [F_0^*, \dots, F_{N-1}^*]^T, \end{aligned} \quad (24)$$

where $F^* = F_{\text{drive}} + F_{\text{brake}}$. The regularisation terms r_δ and r_F chosen must be small enough not to cause any significant distortion of the original problem. The costs of the quality function no longer correspond to the actual quality measure, the lap time t_f , but are artificially increased by the regularisation terms. In order to determine the exact lap

time of the optimised trajectory, the portions of SF in each interval $[s_k, s_{k+1}]$ are evaluated and summed up after the optimisation.

Smoothed control variables usually lead to a higher lap time t_f . Therefore, when the regularisation parameters r_δ and r_F are selected, a compromise must be reached between increasing the value of the cost function by ΔJ , the lap time t_f and smoothing the control variables. For this paper, the regularisation parameters are selected as $r_\delta = 10$ and $r_F = 0.5 \cdot 10^{-8}$. This allows sufficient smoothing of the control variables and, with $\Delta t_f = 0.209$ s and $\Delta J = 0.927$, prevents a significant increase in the lap time and falsification of the MLTP.

6. Simulation results

In this section, we present the simulation results obtained by the suggested trajectory planning for the autonomous development vehicle DevBot of the Roborace racing series. The slightly varied parameters used for vehicle modelling can be found in the Appendix. The implementation is performed in Python 3.7 using the software framework CasADi 3.4.5 [32] and the NLP Solver IPOPT [12] with the linear Solver Mumps. A comparison of the suggested trajectory planning with a minimum curvature trajectory planning is presented in [23].

6.1. Vehicle modelling

In the following, a comparison is made between the vehicle models presented. The effects of the different vehicle models on the race line and the lap times are shown in Figure 6 for two segments of the Berlin Formula E racetrack. In most track sections, there is good agreement between the single track model and the double track model. However, the lap time of the single track model is much shorter.

The accuracy of the optimal solution strongly depends on the chosen discretization length Δs , as it influences both the accuracy of the control discretization as well as the accuracy of the solution of the differential equations. The calculation time t_{NLP} increases significantly for small Δs , while no major increase in accuracy can be observed. Therefore, the discretization step size is set to $\Delta s = 3.0$ m. The computation times from centre line import to trajectory output are approximately 100 s for the single track model and 120 s for the double track model on a laptop computer (Intel i7-4600U @ 2.1 GHz, 12 GB RAM).

A better understanding of the presented lap time differences can be gained by looking at Figure 7. The speed course v shows a good agreement between the models, with a clear deviation visible only between corners 7 and 8. This is due to a different race line choice of the single track model in this section, caused by the overestimation of the traction potential, which will be explained later.

The second row of Figure 7 shows the course of the wheel load transfers Γ_x and Γ_y of the double track model. In direct comparison, the wheel load shift in the longitudinal direction Γ_x is clearly smaller. Therefore, the consideration of Γ_y seems to be more important than Γ_x for motor racing.

Finally, the lower row of Figure 7 shows the course of the maximum acceleration $a_{\text{tot}} = \sqrt{a_x^2 + a_y^2}$ and reveals that the single track model uses significantly higher maximum accelerations a_{tot} than the double track model. The elevations always occur at the

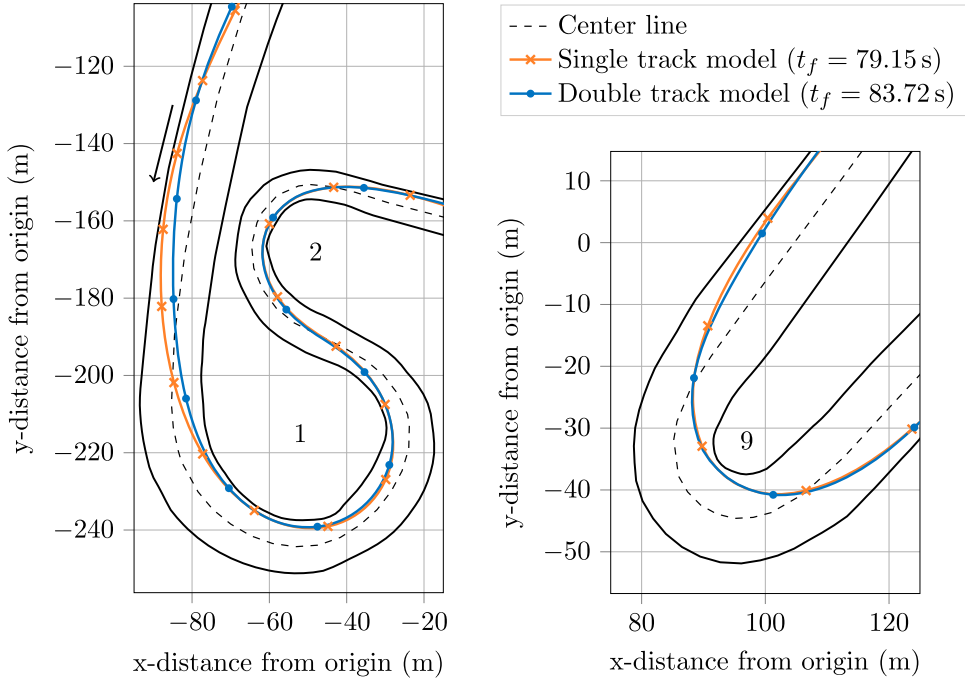


Figure 6. Comparison of the race lines resulting from single track model and double track model for two track sections of the Formula E racetrack in Berlin.

track sections where high lateral wheel load transfer Γ_y can be observed for the double track model. Due to the higher acceleration usage the single track model enables a lap time that is reduced by 4.57 s compared to the double track model.

In order to identify the cause of these differences between the single track model and double track model more precisely, the time-optimal trajectory for the double track model is solved by neglecting the lateral wheel load transfer ($\Gamma_y = 0$). This shows that the consideration of the lateral wheel load shift is responsible for the majority of the time loss (3.60 s). The remainder of the time loss (0.97 s) is due to different kinematic relationships. The consideration of lateral wheel load transfer causes a reduced lateral force potential, because the tyre model used is degressive against the normal force F_z , thus explaining the higher lap time of the double track model. The influence of this degressivity can be quantified as 1.48 s using the simplified tyre model. The remainder of the time delay (2.12 s) caused by consideration of lateral wheel load transfer Γ_y is due to the given distribution of the longitudinal forces F_x . When a race car corners, higher normal forces are produced on the outer wheel, resulting in a higher maximum transferable tyre force. In the case of the static, even distribution of the driving forces on the rear axle, this means that the maximum driving force on the outer wheel is limited by the driving force of the relieved inner wheel.

In order to counteract this restriction, the use of a torque vectoring system is considered. For this vehicle with two separate electric motors on the rear axle, the drive torque of the rear wheels will be distributed individually within the motor limitations. For the extension of the double track model with torque vectoring on the rear axle, the control variable F_{drive}

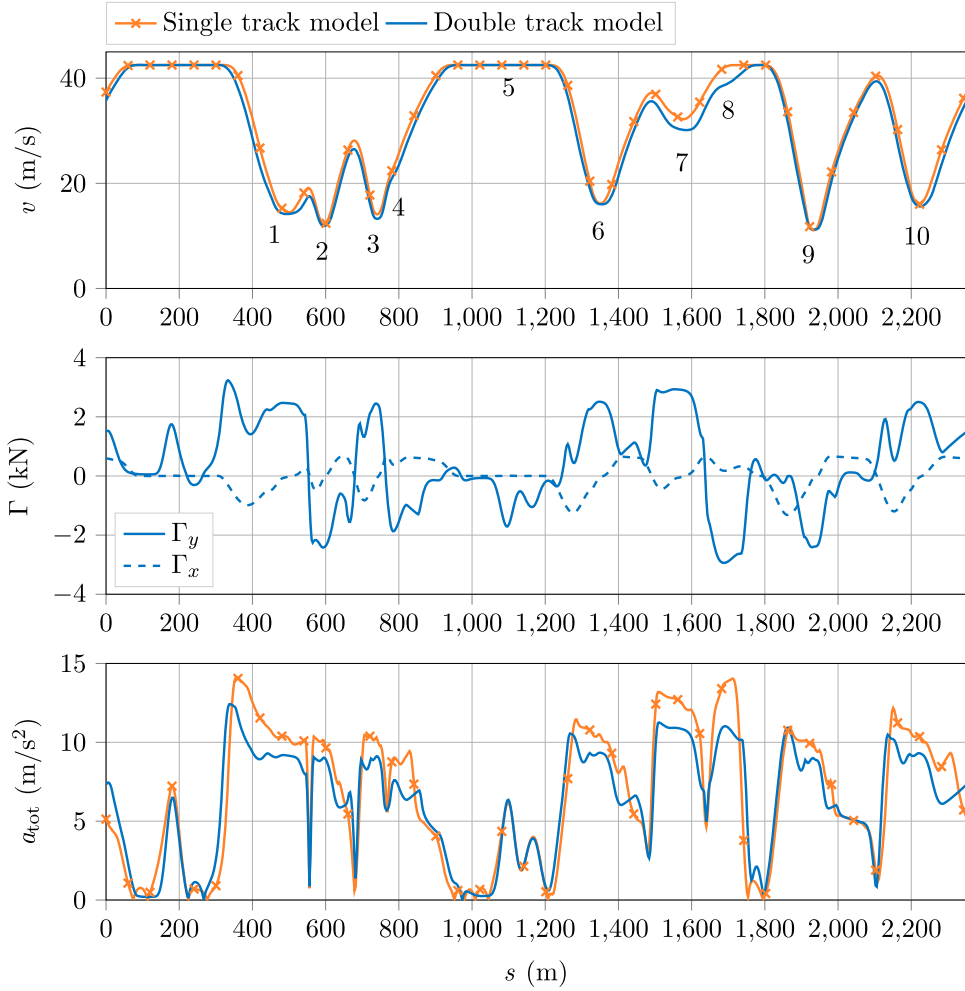


Figure 7. Comparison of the velocity v , wheel load transfers Γ and the total acceleration a_{tot} resulting from single track model and double track model for the Formula E racetrack in Berlin.

is replaced by the two driving forces $F_{drive,rl}$ and $F_{drive,rr}$. The variable force distribution on the rear axle is shown in Figure 8 for the Formula E racetrack in Berlin.

Compared to the even distribution of the driving force $F_{drive}/2$, significant differences between the driving forces at the rear wheels can be observed. It is apparent that $\Delta F_{TV} = F_{drive,rl} - F_{drive,rr}$ is positive in narrow right corners with large lateral wheel load transfer Γ_y (curves 2, 8, 9), while in narrow left corners (curves 1, 3, 6, 7, 10) ΔF_{TV} is negative. Due to this improved dynamic drive force distribution, the outside rear tyre is no longer restricted by the inside tyre and the traction potential of the tyres on the rear axle can be better exploited. The torque vectoring allows the maximum traction potential on both rear tyres to be used at the same time on some sections of the track. This leads directly to higher usable accelerations a_{tot} , which in turn lead to lower lap times. The time saving Δt gained by the introduction of torque vectoring at the rear axle is 1.27 s, which can be enlarged by taking into account variable recuperation power of the electric motors at the rear axle.

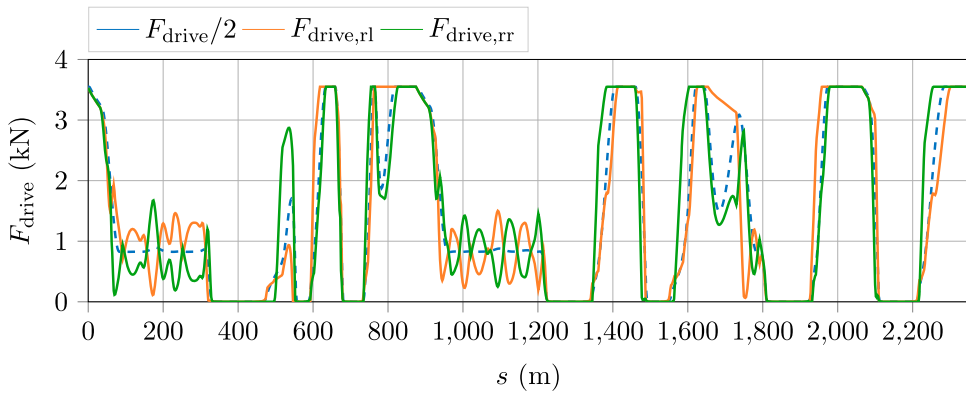


Figure 8. Torque vectoring for the driving forces at the rear axle for the Formula E racetrack in Berlin.

The above investigations therefore clearly show that lateral wheel load transfer is essential for motor racing with high lateral acceleration.

6.2. Variable tyre-road friction coefficients

Variable friction coefficients along the racetrack have a significant impact on the trajectory. First of all, simple scenarios are considered. Figure 9 shows the influence of variable friction coefficients along an artificial racetrack on the course of the race line for the double track model. The friction coefficient is chosen as $\mu = 1.0$, although it is selected differently in the two marked regions. In corner 1, the friction coefficient μ increases linearly from 0.25 on the inside of the corner to 0.75 on the outside. In corner 3, the friction coefficient is greatly reduced and is constant at $\mu = 0.1$ in the marked area. These simple cases allow an exact description of the variable friction coefficient μ with linear equations.

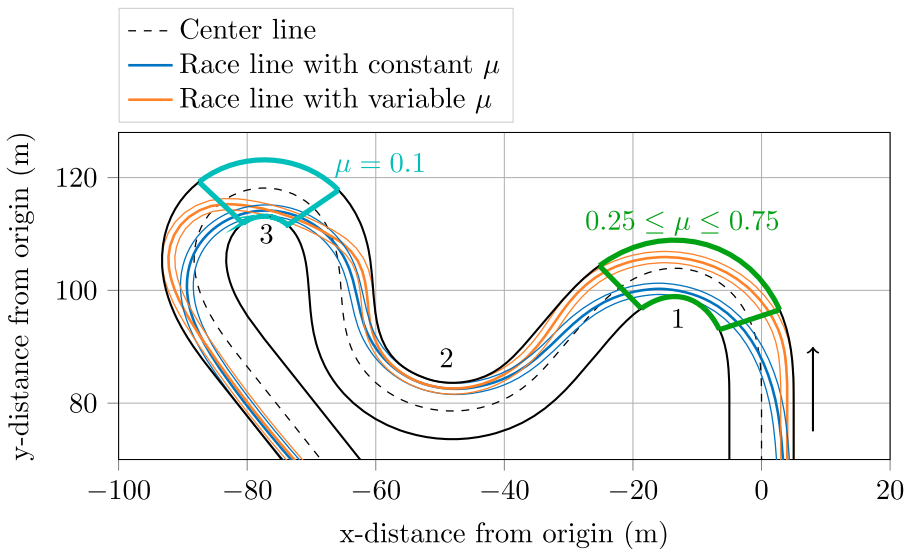


Figure 9. Impact of variable friction coefficients on the race line for an artificial handling track.

In corner 1, a larger corner radius is selected because the friction coefficient in the marked area increases linearly to the outside of the corner. Due to the wheel load transfer, the friction coefficients of the outer tyres are decisive. Consequently, a compromise between a long distance with high friction coefficients and a short distance with low friction coefficients is reached. The locally reduced static friction coefficient $\mu = 0.1$ in corner 3 results in a time-optimised race line with significantly less curvature in the marked zone, since the maximum lateral acceleration is reduced by the reduced traction potential. In addition, a different race line is selected before the zone, promoting a lower curvature of the racing line in the area with a lower friction coefficient. As soon as the front wheels enter the marked zone, it is no longer possible to make significant changes to the driving direction.

In the next step, more realistic friction maps with a discretization area of 0.25 m^2 are considered for the Berlin Track. In order to ensure a sufficiently accurate approximation of the friction map, a discretization length of $\Delta s = 1.0 \text{ m}$ is selected, while the friction coefficients along the normal for each path coordinate s_k are performed by linear combination of 11 gaussian basis functions.

An artificially generated friction map, see Figure A1 in the Appendix, serves as a basis for the subsequent comparison, whereby the range of friction coefficients ($1.0 \pm \Delta\mu$) was varied to simulate small changes of the friction coefficient along the racetrack. Table 1 shows the influence of different friction coefficient ranges on the lap time t_f as well as on the average and maximum deviation of the speed v and the lateral distance to the reference line n . This exemplary friction map shows that even small changes in the friction coefficients along the race track can have a significant influence on the lap time, the velocity and the race line. For example, the maximum lateral deviation of the race line with $\Delta\mu = \pm 0.1$ is already 2.944 m.

However, the methodology presented here also allows strong local changes in the friction coefficients along the racetrack to be taken into account as can be seen in the next example. For this purpose a friction map with two additional areas with no friction at all ($\mu = 0$) is used, see Figure 10. The change in the original race line (see Figure 6) due to the introduction of the friction map is mainly determined by the two areas without friction (blue). The blue area before entering corner 1 is not used because a high lateral acceleration is required in this section. Instead, corner 1 is approached further inwards, which results in a larger race line curvature and thus a lower speed in corner 1. Between corners 2 and 3, an oil track is modelled in the middle of the roadway with a width of 1.5 m. As it turns out, the race line is chosen in such a way that none of the wheels pass over the area with $\mu = 0$.

Table 1. Impact of small changes of the friction coefficient (see friction map in Figure A1 with different $\Delta\mu$) on the lap time t_f , the velocity v and the lateral distance n for the Formula E racetrack in Berlin.

$\Delta\mu$	± 0.02	± 0.04	± 0.06	± 0.08	± 0.10	
Δt_f	0.085	0.188	0.312	0.458	0.625	s
$\text{mean}(\Delta v)$	0.043	0.087	0.134	0.185	0.243	m/s
$\text{max}(\Delta v)$	0.212	0.418	0.619	0.815	1.044	m/s
$\text{mean}(\Delta n)$	0.051	0.208	0.171	0.240	0.308	m
$\text{max}(\Delta n)$	0.414	0.986	1.605	2.278	2.944	m

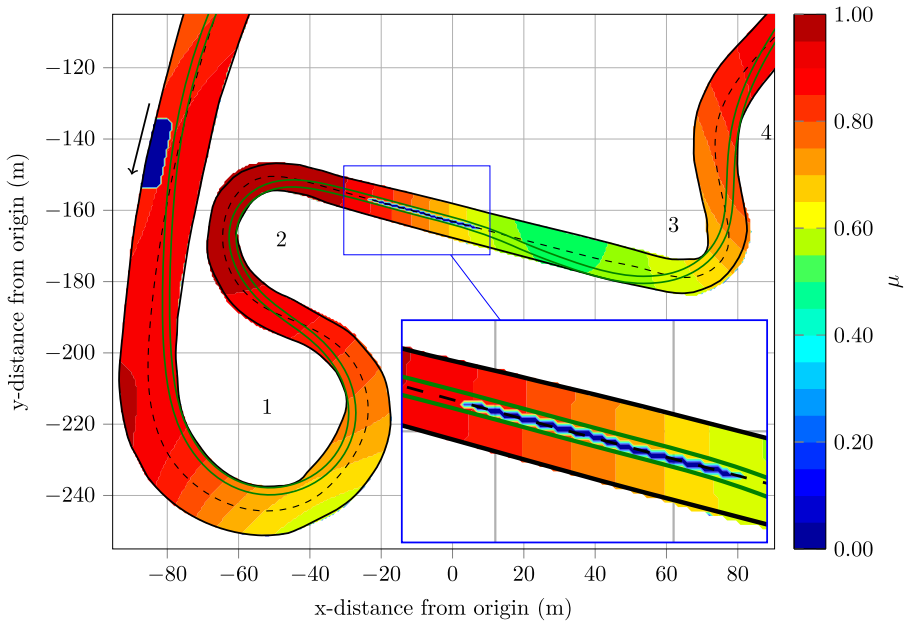


Figure 10. Impact of variable friction coefficients on the race line resulting from double track model for a track section of the Formula E racetrack in Berlin.

Ultimately, the methodology presented for the consideration of variable friction coefficients is proven to be a practical extension, with which the calculation duration does not increase.

7. Conclusion and outlook

In this paper, we have presented a new approach to the planning of a time-optimal trajectory for an autonomous race car. The value of this work lies in a more realistic image of the environmental conditions through the inclusion of the road condition using variable wheel-specific friction coefficients along the racetrack. We have shown that a friction map can be taken into account in the optimal control formulation when using a curvilinear abscissa approach and the arc length of the reference line as independent variable. The quality of the map representation, as well as the numerical effort, are mainly determined by the choice of functions for the approximation of the friction coefficients, as well as by the discretization length of the independent variable. In this context, further investigation should show whether the formulation of the tyre potential at the collocation points allows a greater discretization length and limits the numerical effort. The proposed trajectory planning has proven its practical suitability in first tests on the Roborace car and will be used in the coming racing season in the Roborace competition. In addition, investigations into energy optimal control are likely to be undertaken in the near future. The entire Python code used in the TUM Roborace team for time-optimal global trajectory optimisation will be published under an open source license on GitHub after publication of this paper.¹

Note

1. https://github.com/TUMFTM/global_racetrajectory_optimization.

Acknowledgements

Fabian Christ as the first author developed the presented time-optimal trajectory optimisation in the course of his master's thesis at the Technical University of Munich within the Roborace project. Alexander Wischnewski and Alexander Heilmeyer as his advisors and members of the Roborace project supported this work and contributed to the progress of this work. Boris Lohmann contributed to the conception of the research project and revised the paper critically for important intellectual content. Research was supported by the basic research fund of the Chair of Automotive Technology of the Technical University of Munich. We would also like to thank Leonhard Hermansdorfer and Dieter Pfahl, who provided the centre line extraction and the tool to create realistic friction maps.


Disclosure statement

No potential conflict of interest was reported by the authors.

ORCID

Fabian Christ  <http://orcid.org/0000-0003-0049-1797>

Alexander Wischnewski  <http://orcid.org/0000-0001-6168-8556>

Alexander Heilmeyer  <http://orcid.org/0000-0002-2442-3652>

References

- [1] Kelly DP. Lap time simulation with transient vehicle and tyre dynamics [PhD thesis]. Cranfield University School of Engineering; 2008.
- [2] Casanova D. On minimum time vehicle manoeuvring: the theoretical optimal lap [PhD thesis]. Cranfield University; 2000.
- [3] Dal Bianco N, Bertolazzi E, Biral F, et al. Comparison of direct and indirect methods for minimum lap time optimal control problems. *Vehicle Syst Dyn*. 2018;3(1):1–32.
- [4] Pontryagin LS. Mathematical theory of optimal processes. 4th ed. Boca Raton (FL): Routledge; 2018. (Classics of Soviet mathematics).
- [5] Rao AV, editor. *Astrodynamic 2009: Proceedings of the AAS/AIAA Astrodynamic Specialist Conference; 2009 Aug 9–13; Pittsburgh (PA)*. San Diego (CA): Univelt; 2010. (Advances in the astronautical sciences; 135).
- [6] Dal Bianco N, Lot R, Gadola M. Minimum time optimal control simulation of a GP2 race car. *Proc Inst Mech Eng Part D: J Automobile Eng*. 2017;232(9):1180–1195.
- [7] Lot R, Bianco N. The significance of high-order dynamics in lap time simulations. In: Rosenberger M, Plöchl M, Six K, et al., editors. *The dynamics of vehicles on roads and tracks: proceedings of the 24th symposium of the International Association for Vehicle System Dynamics (IAVSD 2015); 2015 Aug 17–21; Graz, Austria*. Boca Raton (FL): CRC Press; 2016. p. 553–562.
- [8] Lot R, Biral F. A curvilinear abscissa approach for the lap time optimization of racing vehicles. *IFAC Proc Vol*. 2014;47(3):7559–7565.
- [9] Lot R, Dal Bianco N. Lap time optimisation of a racing go-kart. *Vehicle Syst Dyn*. 2015;54(2):210–230.
- [10] Tavernini D, Velenis E, Lot R, et al. The optimality of the handbrake cornering technique. *J Dyn Syst Meas Control*. 2014;136(4):041019.
- [11] Bertolazzi E, Biral F, Da Lio M. Symbolic-numeric efficient solution of optimal control problems for multibody systems. *J Comput Appl Math*. 2006;185(2):404–421.

- [12] Wächter A, Biegler LT. On the implementation of an interior-point filter line-search algorithm for large-scale nonlinear programming. *Math Program.* [2006](#);106(1):25–57.
- [13] Gill PE, Murray W, Saunders MA. SNOPT: an SQP algorithm for large-scale constrained optimization. *SIAM J Optim.* [2002](#);12(4):979–1006.
- [14] Perantoni G, Limebeer DJ. Optimal control for a formula one car with variable parameters. *Vehicle Syst Dyn.* [2014](#);52(5):653–678.
- [15] Nie Y, Faqir O, Kerrigan EC. ICLOCS2: try this optimal control problem solver before you try the rest. 2018 UKACC 12th International Conference on Control (CONTROL); 2018 Sept 5–7; Sheffield, UK. IEEE; 2018. p. 336.
- [16] Limebeer D, Perantoni G, Rao AV. Optimal control of formula one car energy recovery systems. *Int J Control.* [2014](#);4(3):1–16.
- [17] Imani Masouleh M, Limebeer DJN. Optimizing the aero-suspension interactions in a formula one car. *IEEE Trans Control Syst Technol.* [2016](#);24(3):912–927.
- [18] Limebeer DJN, Perantoni G. Optimal control of a formula one car on a three-dimensional track – Part 2: optimal control. *J Dyn Syst Meas Control.* [2015](#);137(5):051019.
- [19] Patterson MA, Rao AV. GPOPS-II. *ACM Trans Math Softw.* [2014](#);41(1):1–37.
- [20] Gundlach I, Konigorski U, Hoedt J. Zeitoptimale Trajektorienplanung für automatisiertes Fahren im fahrdynamischen Grenzbereich. *VDI Ber.* [2017](#);2292:223–234.
- [21] van Koutrik S. Optimal control for race car minimum time maneuvering [Master's thesis]. Delft University of Technology; 2015.
- [22] Kapania NR, Subosits J, Gerdes JC. A sequential two-step algorithm for fast generation of vehicle racing trajectories. *J Dyn Syst Meas Control.* [2016 Apr](#);138(9):091005.
- [23] Heilmeier A, Wischnewski A, Hermansdorfer L, et al. Minimum curvature trajectory planning and control for an autonomous race car. *Vehicle Syst Dyn.* [2019](#);25:1–31.
- [24] Milliken DL. Race car vehicle dynamics: problems, answers and experiments (SAE-R 280). Warrendale (PA): SAE International; [2003](#).
- [25] Pfeffer P, Harrer M. *Lenkungsbandbuch*. Wiesbaden: Springer Fachmedien Wiesbaden; [2013](#).
- [26] Trzesniowski M. *Rennwagentchnik*. Wiesbaden: Springer Fachmedien Wiesbaden; [2014](#).
- [27] Mitschke M, Wallentowitz H. *Dynamik der Kraftfahrzeuge*. Wiesbaden: Springer Fachmedien Wiesbaden; [2014](#).
- [28] Khaleghian S, Emami A, Taheri S. A technical survey on tire-road friction estimation. *Friction.* [2017](#);5(2):123–146.
- [29] Hermansdorfer L, Betz J, Markus L. A concept for estimation and prediction of the tire-road friction potential for an autonomous racecar. 2019 IEEE 22nd Intelligent Transportation Systems Conference (ITSC); 2019 Oct 27–30; Auckland, New Zealand. IEEE; 2019. p. 1490–1495.
- [30] Diehl M, Gros S. Numerical optimal control: Unpublished manuscript; 2017.
- [31] Andersson J. A general-purpose software framework for dynamic optimization [PhD thesis]. KU Leuven; 2013.
- [32] Andersson JAE, Gillis J, Horn G, et al. CasADi: a software framework for nonlinear optimization and optimal control. *Math Program Comput.* [2018](#);20(3):1655.
- [33] Betts JT. *Practical methods for optimal control and estimation using nonlinear programming*. Philadelphia (PA): Society for Industrial and Applied Mathematics; [2010](#).

Appendices

Appendix 1. Vehicle and tyre data

Table A1. Vehicle parameters used for single track and double track models.

Symbol	Description	Value
ρ	Air density	1.2041 kg/m ³
g	Gravitational acceleration	9.81 m/s ²
m	Vehicle mass	1200 kg
l	Wheelbase	2.9 m
l_f	Distance of the mass centre from the front axle	1.5 m
l_r	Distance of the mass centre from the rear axle	1.4 m
tw_f	Track width at front axle	1.6 m
tw_r	Track width at rear axle	1.5 m
b	Vehicle width	2.0 m
h_{cog}	Center of mass height	0.4 m
J_{zz}	Moment of inertia about the z-axis	1260 kg m ²
A	Frontal area	1.0 m ²
c_d	Drag coefficient	1.4
$c_{l,f}$	Downforce coefficient at front axle	2.4
$c_{l,r}$	Downforce coefficient at rear axle	3.0
f_r	Rolling resistance coefficient	0.010
k_{drive}	Drive force distribution (fraction at front axle)	0.0
k_{brake}	Brake force distribution (fraction at front axle)	0.7
k_{roll}	Roll moment distribution (fraction at front axle)	0.5
P_{max}	Maximum engine power	270 kW
$F_{\text{drive,max}}$	Maximum driving force	7100 N
$F_{\text{brake,max}}$	Maximum braking force	−20,000 N
δ_{max}	Maximum steer angle	0.4 rad
T_{drive}	Time constant for drive	1.0 s
T_{brake}	Time constant for brake	1.0 s
T_{δ}	Time constant for steering	1.0 s
r_{δ}	Regularization parameter for steering angle change	10
r_F	Regularization parameter for longitudinal force change	0.5
v_{max}	Maximum velocity	42.5 m/s

Table A2. Parameters used for magic formula tyre models.

tyre	B	C	E	$F_{z,0}$	ϵ
front	10	2.35	1	3000	−
rear	9.5	2.60	1	3000	−
front (extended)	9.62	2.59	1	3000	−0.0813
rear (extended)	8.62	2.65	1	3000	−0.1263

Appendix 2. Friction map

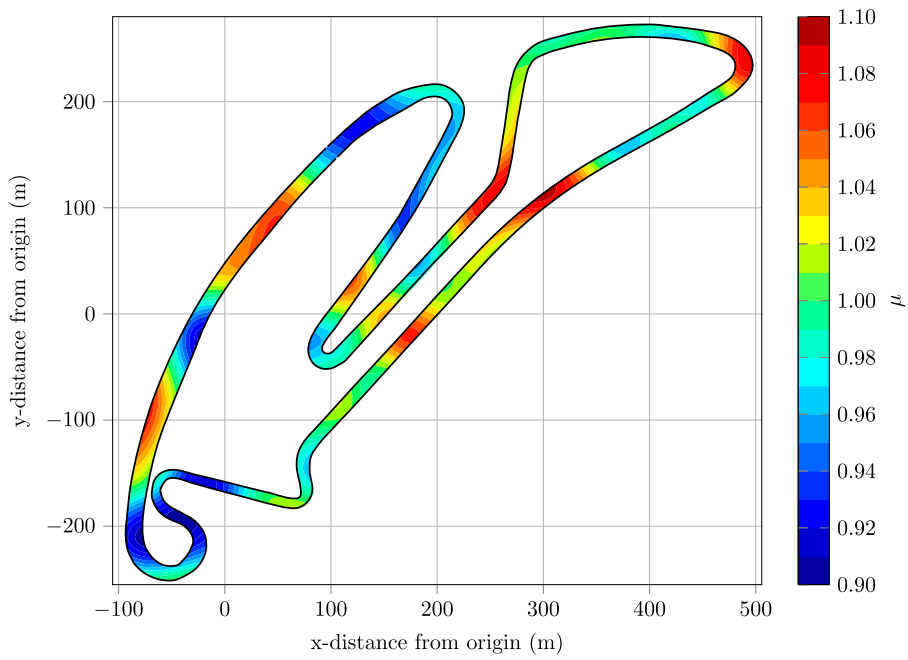


Figure A1. Artificial friction map for the Formula E racetrack in Berlin with a variation of the friction coefficients of $\Delta\mu = \pm 0.1$.